Battery Materials

International Edition: DOI: 10.1002/anie.201503477
German Edition: DOI: 10.1002/ange.201503477

Enhancement of Sodium Ion Battery Performance Enabled by Oxygen Vacancies**

*Yang Xu, Min Zhou, Xin Wang, Chengliang Wang, Liying Liang, Fabian Grote, Minghong Wu, Yan Mi, and Yong Lei**

Abstract: *The utilization of oxygen vacancies (OVs) in sodium ion batteries (SIBs) is expected to enhance performance, but as yet it has rarely been reported. Taking the MoO_{3-x} nanosheet anode as an example, for the first time we demonstrate the benefits of OVs on SIB performance. Moreover, the benefits at deep-discharge conditions can be further promoted by an ultrathin Al_2O_3 coating. A series of measurements show that the OVs increase the electric conductivity and Na-ion diffusion coefficient, and the promotion from ultrathin coating lies in the effective reduction of cycling-induced solid-electrolyte interphase. The coated nanosheets exhibited high reversible capacity and great rate capability with the capacities of 283.9 ($50\ mA\ g^{-1}$) and 179.3 $mAh\ g^{-1}$ ($1\ A\ g^{-1}$) after 100 cycles. This work may not only arouse future attention on OVs for sodium energy storage, but also open up new possibilities for designing strategies to utilize defects in other energy storage systems.*

Defects such as oxygen vacancies (OVs) often dominate the electric and chemical properties of transition-metal oxides, and thus they play a crucial role in a wide range of applications.[1] In lithium ion batteries (LIBs), OVs can trigger changes in the electronic structure of metal oxides, so affecting the energetics for electron and ion transport.[2] Their presence at the electrode/electrolyte interface not only can possibly facilitate the phase transition experienced in lithiation by modified surface thermodynamics, but also well preserve the integrity of the electrode surface morphology.[3] The effect of OVs on cyclability and rate capacity has been widely reported in LIBs;[4] however, as far as we know, the relevant study on sodium ion batteries (SIBs) is currently missing. Such kind of knowledge is of great importance to develop the large-scale energy storage devices.

SIBs have recently come again into focus as the important alternative energy storage devices owing to the low cost of Na associated with its natural abundance and decent energy density bestowed by its similar chemical nature to Li. Many electrode materials for LIBs have been investigated as drop-in replacements for SIBs.[5] Owing to the difference in the standard electrochemical potential for Na (3.04 V) and Li (2.71 V), the reduction of voltage can be expected in the Na system when the same chemistry (redox species and host crystal structures) with the Li system is used. The reduction becomes even more significant as Na content in the host structure increases because of the different chemistry from the Na system, for which the larger size of Na-ion (1.02 Å) relative to Li-ion (0.76 Å) is generally believed to be responsible.[6] For example, MoO_3 is generally considered as a LIB cathode but delivers comparable capacity as SIB anode at deep-discharge condition (< 0.1 V vs. Na/Na^+).[7] To properly utilize OVs in such a low-voltage system, decomposition of electrolyte (both solvent and salt) and formation of solid–electrolyte interphase (SEI) have to be considered. SEI can largely change the solid–liquid interface, and thus interfere with the function of the OVs, leading to poor coulombic efficiency (CE) and overall capacity loss. It is even more critical for NIBs owing to the higher chemical reactivity of Na over Li.[8] Therefore, using OVs requires combination with other strategy to overcome the adverse effects of SEI and maximize their advantages.

The proper functioning of OVs at the deep-discharge condition requires the reduction of cycling-induced SEI. A thin surface coating by atomic layer deposition (ALD) has proved to be effective regarding the above-mentioned issue.[9] The thin layer can act as a mechanically stable kinetic barrier against electron transfer to the organic carbonate molecules of the electrolytes, thus preventing the formation of excessive amounts of SEI and suppressing the side reactions. Meanwhile, ALD enables a precisely controlled thin coating with pinhole free conformal morphology. A recent work reported that a thin ALD coating of Al_2O_3 can react with Na-ions to irreversibly form a mechanically durable Na-Al-O layer that acts as an ion transport channel and improves Na-ion diffusion into the electrode through its whole surface.[10] This observation inspires us to use thin Al_2O_3 coating as a suitable strategy to ensure the proper functioning of OVs.

In this work, we demonstrate, for the first time, the effect of OVs on sodium energy storage by using MoO_{3-x} nanosheets as anodes. The nanosheets exhibited improved electro-

[*] Dr. Y. Xu,[+] Dr. M. Zhou,[+] Dr. C. L. Wang, L. Y. Liang, F. Grote, Y. Mi, Prof. Y. Lei
Institute für Physics & IMN MacroNano (ZIK)
Technische Universität Ilmenau
Prof-Schemidt-Strasse 26, 98693 Ilmenau (Germany)
E-mail: yong.lei@tu-ilmenau.de
X. Wang, Dr. M. Wu, Prof. Y. Lei
Institute of Nanochemistry and Nanobiology
School of Environment and Chemical Engineering
Shanghai University, Shanghai, 200444 (P.R. China)
[+] These authors contributed equally to this work.

[**] This work was financially supported by the European Research Council (ThreeDsurface: 240144), BMBF (ZIK-3DNanoDevice: 03Z1MN11), Volkswagen-Stiftung (Herstellung funktionaler Oberflächen: I/83 984), and the Shanghai Thousand Talent Plan and Innovative Research Team (No. IRT13078). We thank Mr. Yong Yan for his assistant of the XRD measurement. We also thank Dr. Xiaodong Zhang for his assistant of the XPS measurement.

Supporting information for this article is available on the WWW under http://dx.doi.org/10.1002/anie.201503477.

chemical performance comparing to the MoO_3 counterpart owing to the increased electric conductivity and Na-ion diffusion coefficient deriving from the existence of OVs. By coating an ultrathin Al_2O_3 layer on the electrodes, the function of OVs at the deep-discharge condition was further promoted, giving rise to high reversible capacity and great rate capability over long-term cycling.

The X-ray diffraction (XRD) pattern of the as-prepared nanosheets (Figure 1a) can be assigned to the orthorhombic

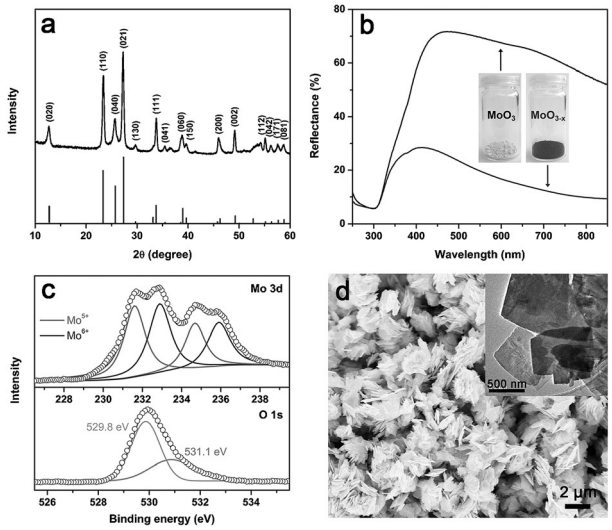

Figure 1. a) XRD pattern of the as-prepared MoO_{3-x} nanosheets. b) UV/Vis DRS spectra of the MoO_{3-x} and MoO_3 sample with corresponding photographs. c) Mo 3d and O 1s XPS spectra and d) SEM (inset: TEM) image of the sample.

phase (JCPDS No. 5-0508). Although it is not distinguishable from that of MoO_3 (Supporting Information, Figure S1a), the exhibited intense blue color (b-Mo hereafter; comparison shown in the inset of Figure 1b) was quite stable in air and can remain unchanged for several months. It changed to white (inset of Figure 1b, w-Mo hereafter) after annealing in air. Both facts strongly indicate the existence of OVs.[11] The UV/Vis diffuse reflectance spectroscopy (DRS) spectrum shows strong light absorption in the visible light region (350–700 nm, Figure 1b). Such a blue color originates from the intervalence charge-transfer transition between Mo^V and Mo^{VI} that coexist in the nanosheets.[12] X-ray photoelectron spectroscopy (XPS; Figure 1c; Supporting Information, Figure S2a) and energy-dispersive X-ray spectroscopy measurement (EDX; Supporting Information, Figure S2c) reveal the existence of only Mo and O. The Mo 3d spectrum shows two sets of doublets that are ascribed to Mo^V and Mo^{VI}. The O 1s spectrum provides auxiliary evidence of the OVs, where the peak at 529.8 eV belongs to Mo-O-Mo bonds and the one at 531.1 eV is due to a high number of defect sites with a low oxygen coordination.[13] Scanning electron microscopy (SEM) image (Figure 1d) shows two-dimensional (2D) nanosheets on a large scale with the diameter ranging from 400 nm to 2 μm and thickness of 20–30 nm. Transmission electron microscopy (TEM) image (inset of Figure 1d) confirms the shape of 2D nanosheets, and the HRTEM (Supporting Information, Figure S2b) image shows clear lattice fringes, verifying the single-crystalline nature of the nanosheets.

To demonstrate the benefits of OVs, five samples denoted as b-Mo, w-Mo, b-Mo-4Al, b-Mo-8Al, and w-Mo-4Al with the number indicating ALD cycles were tested as SIB anodes based on the existence of OVs and Al_2O_3 coating thickness (ca. 1 Å per cycle). EDX elemental mapping on the b-Mo-4Al anode (Supporting Information, Figure S3) clearly shows the uniform Al_2O_3 coating on electrode surface. The anodes showed similar cyclic voltammetry (CV) curves (Supporting Information, Figure S4) with a redox pair of 0.71 (anodic)/0.22 V (cathodic) became pronounced after the first cycle, indicating the reversible insertion/extraction of Na ion.[7] However, with the existence of OVs and ultrathin coating, the retention of the anodic peak current is significantly increased (Supporting Information, Figure S4f). The charge–discharge profiles (Figure 2a; Supporting Information, Figure S4) are in agreement with the corresponding CV results, and the ex situ XRD measurements revealed that the sodiation reaction is an insertion reaction (Supporting Information, Figure S5). Analysis of cycling performance (Figure 2b) and CE (Figure 2c) allows us to draw the following conclusions. 1) With OVs, b-Mo exhibited higher capacities of 254.0 (10th), 139.9 (50th), and 100.1 $mAh\,g^{-1}$ (100th), compared to w-Mo. 2) The coated anodes displayed increased capacities and better retention comparing to their uncoated counterparts. The capacities of 123.9 (w-Mo-4Al), 254.1 (b-Mo-4Al), and 283.9 $mAh\,g^{-1}$ (b-Mo-8Al) were obtained after 100 cycles. A higher CE of the first 20 cycles (>95% after 5 cycles; inset of Figure 2c) is responsible for the higher capacity and better cyclability. 3) The magnitude of the improvement after coating is more significant with OVs than without OVs, indicating the coating facilitates OV function at the deep-discharge condition. 4) The thickness of Al_2O_3 can be adjusted to optimize the properties. The b-Mo-8Al anode delivered the capacities of 385.1 (10th), 319.2

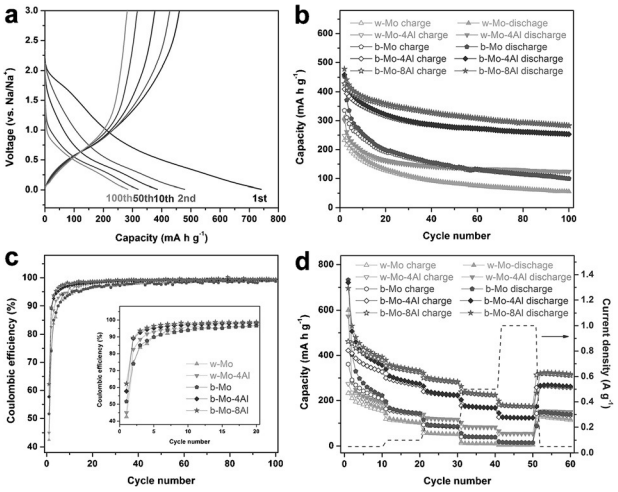

Figure 2. a) Charge–discharge profiles of the b-Mo-8Al anode. b) Cycling performance (starting from the second cycle) and c) CE of the anodes at the rate of 50 $mA\,g^{-1}$. d) Rate capability in a current density range of 50 $mA\,g^{-1}$–1 $A\,g^{-1}$.

(50th), and 283.9 mAh g^{-1} (100th) with the CE reaching 95% after only 4 cycles and remaining over 98% after 12 cycles. Comparison of rate capability (Figure 2d) shows the same trends as in reversible capacity. Higher capacities were obtained from b-Mo over w-Mo at all rates. Coated anodes delivered higher capacities than their uncoated counterparts and more significant enhancement is achieved with OVs. Among all, b-Mo-8Al exhibited the best rate capability of about 230 (0.5 A g^{-1}) and about 180 mAh g^{-1} (1 A g^{-1}). All the results demonstrate the benefits of the OVs that can be further promoted by ultrathin Al_2O_3 coating. Compared to w-Mo-4Al, b-Mo delivered higher capacity only at lower rates, which leads us to investigate the coating-promoted benefits of OVs at higher rates.

Cycling performance of the anodes with OVs at the rate of 0.2, 0.5 and 1 A g^{-1} is shown in Figure 3. Without coating, less

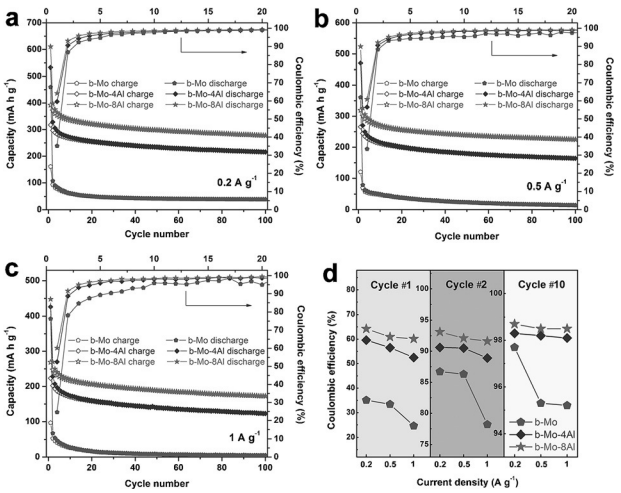

Figure 3. Cycling performance of the anodes with OVs at the rate of a) 0.2, b) 0.5, and c) 1 A g^{-1}. d) Comparison of the CE at different rates.

than 40 mAh g^{-1} retained after 100 cycles at all rates. In contrast, the b-Mo-4/8Al anode delivered significantly increased capacities of 216.3/278.5 (0.2 A g^{-1}), 164.5/225.5 (0.5 A g^{-1}) and 123.3/179.3 mAh g^{-1} (1 A g^{-1}). It is worth noting that similar improvement can be observed from w-Mo-4Al (Supporting Information, Figure S6) but with less prominent capacity increasing without OVs. Such comparison once again confirms the benefits of OVs on cyclability at higher rates. Figure 3d summarizes the CE of three different cycles, where, for the same cycle, it generally decreases with increasing rate. The numbers were substantially improved after coating, which plays a fatal role on the long-term cyclability. More importantly, the coating alleviates the CE reduction caused by increasing rate, which explains the higher capacity retention of the coated anodes at higher rates.

The improved performance of b-Mo over w-Mo can be attributed to the increased electronic conductivity (that is, reduced impedance) and Na-ion diffusion, which can be verified by electrochemical impedance spectroscopy (EIS) measurement. Table 1 summarizes the parameters obtained from the Nyquist plots (Supporting Information, Figure S7)

Table 1: Physicochemical properties measured and calculated from EIS.[a]

Sample	R_s [Ω] before	R_{ct} [Ω] before	R_s [Ω] after	R_{ct} [Ω] after	D_{Na} [cm^2 s^{-1}]
w-Mo	6.26	175.90	7.87	546.60	8.28×10^{-12}
b-Mo	7.65	115.20	7.76	426.10	4.36×10^{-11}

[a] EIS = Electrochemical impedance spectroscopy. R_s = electrolyte resistance, R_{ct} = charge-transfer resistance.

before and after 100 cycles at 50 mA g^{-1}. Two anodes show similar electrolyte resistance (R_s) due to the same electrolyte. However, b-Mo exhibits much lower charge-transfer resistance (R_{ct}), indicating that the electron transport can be significantly improved by OVs during the entire process. After cycling, b-Mo possesses higher Na-ion diffusion coefficient (D_{Na}) calculated from the low frequency Warburg contribution (Supporting Information, Figure S7b).[14] In other words, increased Na-ion diffusion deriving from OVs can be maintained even after long-term cycling.

To illustrate the promoting effect of ultrathin Al_2O_3 coating on OVs, EIS and XPS measurements were carried out on the anodes with OVs cycled at 0.2 A g^{-1}. As shown in Figure 4a and the Supporting Information, Figure S8, the

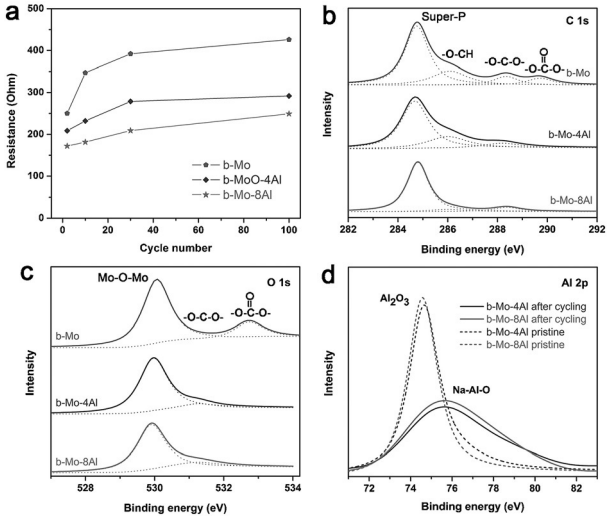

Figure 4. a) Comparison of R_{ct} of the coated anodes during cycling. b) C 1s, c) O 1s, and d) Al 2p XPS spectra of the anodes after 100 cycles at 0.2 A g^{-1}.

consistently lower resistance of b-Mo-4/8Al during cycling agrees well with the CE trend and signals lower rates of SEI formation. It demonstrates that Al_2O_3 coating effectively improves the kinetics at solid-liquid interface at deep-discharge condition, leading to the higher reversible capacity and better retention at higher rates. XPS results reveal the surface information regarding cycling-induced SEI. In the C 1s (Figure 4b), O 1s (Figure 4c), and Na 2s spectra (Supporting Information, Figure S9), the peaks associated with the electrolyte decomposition products (for example, alkyl, alkoxy, carbonate, ether)[15] show less intensity from the coated anodes. The results support our assumption that Al_2O_3

layer can act as a mechanically stable substitute for SEI to suppress electrolyte decomposition and inhibit the formation of thick SEI,[16] thus promoting the function of the OVs at the deep-discharge condition. Moreover, the fact that strong Al signal is still detected after 100 cycles (Figure 4d) confirms that the amount of SEI on the electrode surface is relatively low.

In summary, taking ultrathin Al_2O_3-coated MoO_{3-x} nanosheets as example, we have demonstrated the crucial role of OVs in sodium energy storage, which is verified by a series of measurements, including long-term cycling, EIS, and XPS. In detail, OVs can enhance the electric conductivity and Na-ion diffusion coefficient; meanwhile Al_2O_3 coating can reduce the cycling-induced SEI formation, facilitating the proper functioning of OVs at the deep-discharge condition. Through the combination of OVs and ultrathin surface coating, the b-Mo-8Al anode exhibited high reversible capacity and great rate capability over long-term cycling, delivering capacities of 283.9 ($50\,mA\,g^{-1}$) and $179.3\,mAh\,g^{-1}$ ($1\,A\,g^{-1}$) after 100 cycles. This work aims at providing suitable strategy to take full advantages of OVs in upgrading SIB properties and may open up new possibilities of defects for new energy storage systems.

Experimental Section

Material synthesis and electrode fabrication: MoO_{3-x} nanosheets were obtained by oxidizing Mo powders in H_2O_2 followed by solvothermal treatment in absolute ethanol. Electrodes were fabricated by mixing active material, poly(vinylidenedifluoride) (PVDF), and Super P at a weight ratio of 80:10:10, coated uniformly on Cu foils, and dried at 110°C under vacuum. Al_2O_3 was deposited on the as-prepared electrodes using atomic layer deposition. Further experimental details can be found in Supporting Information.

Keywords: alumina · molybdenum · nanomaterials · oxygen vacancies · sodium ion batteries

How to cite: *Angew. Chem. Int. Ed.* **2015**, *54*, 8768–8771
Angew. Chem. **2015**, *127*, 8892–8895

[1] a) X. B. Chen, L. Liu, P. Y. Yu, S. S. Mao, *Science* **2011**, *331*, 746–750; b) Y. F. Sun, S. Gao, F. C. Lei, Y. Xie, *Chem. Soc. Rev.* **2015**, *44*, 623–636; c) C. H. Ahn, J.-M. Triscone, J. Mannhart, *Nature* **2003**, *424*, 1015–1018.

[2] R. Schaub, E. Wahlström, A. Rønnau, E. Lægsgaard, I. Stensgaard, F. Besenbacher, *Science* **2003**, *299*, 377–379.

[3] M. V. Ganduglia-Pirovano, J. Sauer, *Phys. Rev. B* **2004**, *70*, 045422.

[4] a) P. V. Sushko, K. M. Rosso, J.-G. Zhang, J. Liu, M. L. Sushko, *Adv. Funct. Mater.* **2013**, *23*, 5530–5535; b) J.-Y. Shin, J. H. Joo, D. Samuelis, J. Maier, *Chem. Mater.* **2012**, *24*, 543–551.

[5] a) N. Yabuuchi, K. Kobota, M. Dahbi, S. Komaba, *Chem. Rev.* **2014**, *114*, 11636–11682; b) M. D. Slater, D. H. Kim, E. Lee, C. S. Johnson, *Adv. Funct. Mater.* **2013**, *23*, 947–958; c) C. L. Wang, Y. Xu, Y. G. Fang, M. Zhou, L. Y. Liang, S. Singh, H. P. Zhao, A. Schober, Y. Lei, *J. Am. Chem. Soc.* **2015**, *137*, 3124–3130.

[6] a) S. P. Ong, V. L. Chevrier, G. Hautier, A. Jain, C. Moore, S. Kim, X. H. Ma, G. Ceder, *Energy Environ. Sci.* **2011**, *4*, 3680–3688; b) C. Delmas, J.-J. Braconnier, C. Fouassier, P. Hagenmuller, *Solid State Ionics* **1981**, *3–4*, 165–169; c) Y. Xu, E. M. Lotfabad, H. L. Wang, B. Farbod, Z. W. Xu, A. Kohandehghan, D. Mitlin, *Chem. Commun.* **2013**, *49*, 8973–8975.

[7] S. Hariharan, K. Saravanan, P. Balaya, *Electrochem. Commun.* **2013**, *31*, 5–9.

[8] a) A. Darwiche, C. Marino, M. T. Sougrati, B. Fraisse, L. Stievano, L. Monconduit, *J. Am. Chem. Soc.* **2012**, *134*, 20805–20811; b) X. Xia, J. R. Dahn, *J. Electrochem. Soc.* **2012**, *159*, A515–A519.

[9] X. B. Meng, X. Q. Yang, X. L. Sun, *Adv. Mater.* **2012**, *24*, 3589–3615.

[10] X. G. Han, Y. Liu, Z. Jia, Y.-C. Chen, J. Y. Wan, N. Weadock, K. J. Gaskell, T. Li, L. B. Hu, *Nano Lett.* **2014**, *14*, 139–147.

[11] H. F. Cheng, T. Kamegawa, K. Mori, H. Yamashita, *Angew. Chem. Int. Ed.* **2014**, *53*, 2910–2914; *Angew. Chem.* **2014**, *126*, 2954–2958.

[12] a) Y. A. Yang, Y. W. Cao, B. H. Loo, J. N. Yao, *J. Phys. Chem. B* **1998**, *102*, 9392–9396; b) L. Zheng, Y. Xu, D. Jin, Y. Xie, *Chem. Mater.* **2009**, *21*, 5681–5690.

[13] a) W. T. Bi, C. M. Ye, C. Xiao, W. Tong, X. D. Zhang, W. Shao, Y. Xie, *Small* **2014**, *10*, 2820–2825; b) J. Y. Gan, X. H. Lu, J. H. Wu, S. L. Xie, T. Zhai, M. H. Yu, Z. S. Zhang, Y. C. Mao, S. C. I. Wang, Y. Shen, Y. X. Tong, *Sci. Rep.* **2013**, *3*, 1021.

[14] Y. G. Wang, H. M. Liu, K. X. Wang, H. Eiji, Y. R. Wang, H. S. Zhou, *J. Mater. Chem.* **2009**, *19*, 6789–6795.

[15] a) V. Etacheri, U. Geiger, Y. Gofer, G. A. Roberts, I. C. Stefan, R. Fasching, D. Aurbach, *Langmuir* **2012**, *28*, 6175–6184; b) L. W. Ji, M. Gu, Y. Y. Shao, X. L. Li, M. H. Engelhard, B. W. Arey, W. Wang, Z. M. Nie, J. Xiao, C. M. Wang, J.-G. Zhang, J. Liu, *Adv. Mater.* **2014**, *26*, 2901–2908; c) V. Etacheri, O. Haik, Y. Goffer, G. A. Roberts, I. C. Stefan, R. Fasching, D. Aurbach, *Langmuir* **2012**, *28*, 965–976.

[16] a) E. M. Lotfabad, P. Kalisvaart, K. Cui, A. Kohandehghan, M. Kupsta, B. Olsen, D. Mitlin, *Phys. Chem. Chem. Phys.* **2013**, *15*, 13646–13657; b) H. T. Nguyen, M. R. Zamfir, L. D. Duong, Y. H. Lee, P. Bondavalli, D. Pribat, *J. Mater. Chem.* **2012**, *22*, 24618–24626; c) E. M. Lotfabad, P. Kalisvaart, A. Kohandehghan, K. Cui, M. Kupsta, B. Farbod, D. Mitlin, *J. Mater. Chem. A* **2014**, *2*, 2504–2516; d) A. L. Lipson, K. Puntambekar, D. J. Comstock, X. B. Meng, M. L. Geier, J. W. Elam, M. C. Hersam, *Chem. Mater.* **2014**, *26*, 935–940; e) A. Kohandehghan, P. Kalisvaart, K. Cui, M. Kupsta, E. Memarzadeh, D. Mitlin, *J. Mater. Chem. A* **2013**, *1*, 12850–12861; f) Y. S. Jung, A. S. Cavanagh, L. A. Riley, S. H. Kang, A. C. Dillon, M. D. Groner, S. M. George, S. H. Lee, *Adv. Mater.* **2010**, *22*, 2172–2176.

Received: April 16, 2015
Published online: June 25, 2015

